Conference Proceedings

EuroSun 2014
Aix-les-Bains (France), 16 - 19 September 2014

Water adsorption on zeolites for solar heat storage: modeling and experimental analysis of the reactor

Parfait Tatsidjodoung[1], Nolwenn Le Pierrès[1], Julien Heintz[2], Davy Lagre[2], Lingai Luo[3]

[1] LOCIE laboratory, Université de Savoie CNRS, Le Bourget du Lac (France)

[2] CETIAT, Lyon-Villeurbanne (France)

[3] LTN laboratory, Université de Nantes CNRS, Nantes (France)

Abstract

This paper presents a study of the evolution of a zeolite sorption vessel for heat storage, using a 1D mathematical model and an experimental bench. The test bench and the main model hypothesis and equations are presented in this paper. The model involves coupled heat and mass transfers inside the reactive porous bed and is used to study the humidity and the temperature of the flowing air at the reactor outlet during both charging and discharging phases. The simulation results fit correctly the experimental results, thus this model could be used to simulate the reactor evolution. The results show that the temperature reached by the air exiting the storage reactor (>55°C) under typical operating conditions that could be observed in a building are appropriate for building heating. The desorption of the reactor at a temperature as low as 120°C is possible, thus the use of solar collectors to heat up the reactor during the charging phase is possible, even though a desorption at a temperature higher than 150°C will allow a higher storage density of the system.

Keywords: sorption, zeolite, storage, modeling, experimentation.

1. Introduction

The mismatch between sunny and heating periods leads to consider heat storage as a solution for solar thermal energy recovery to fulfill heating demands for thermal comfort in buildings. To this end, solid/gas sorption based systems are potentially good candidates (Tatsidjodoung et al., 2013; Yu et al., 2013). These systems can achieve interesting energy densities (between 100 and 250 kWh/kg sorbent (Yu et al., 2013)) and allow to avoid heat losses during storage (heat is stored in the form of a chemical potential). In this study, a solid/gas heat storage reactor filled with zeolite-13X beads is considered. Air flowing through the bed causes the hydration or dehydration of the zeolite, thus the corresponding exothermal adsorption and endothermal desorption processes allow the storage of heat in this reactor. The principle of the charging and discharging phases are presented in Figure 1. The final aim of this project is to evaluate the performances of this type of reactor in the framework of solar heat storage for building heating purposes. The temperature of the hot air used during the charging phase should be reached by solar collectors and the warm air generated during the discharging phase should be at sufficiently high temperature to fit the building needs. In this paper, the modeling and experimental results obtained on a zeolite reactor are presented and analyzed.

Selection and/or peer review under responsibility of EuroSun2014 Scientific Committee
doi:10.18086/eurosun.2014.10.20 Available at http://proceedings.ises.org

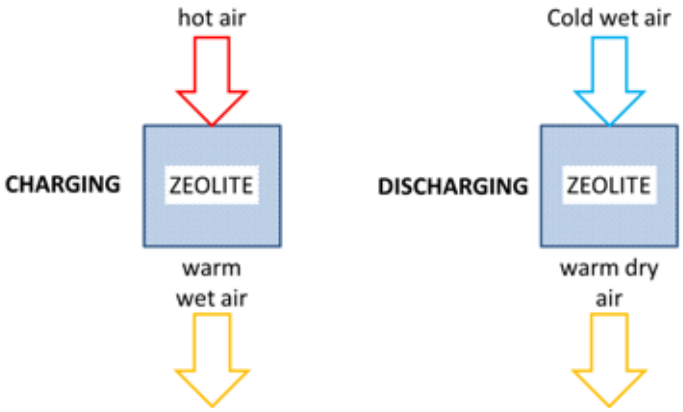

Fig. 1 : Principle of the storage charging and discharging phases

2. Model

2.1. Model assumptions

The one-dimensional model describing mainly air and zeolite beads temperatures and humidities as a function of position and time, is primarily based on the following assumptions:

- the zeolite beads size and porosity, and the bed porosity are supposed uniform;
- the water vapor and the humid air behave as ideal gases;
- radiative heat transfer between solid and gas phases is negligible compared to convective heat transfer ;
- mass diffusion in a direction other than that of the flow is neglected compared to convective transport;
- zeolite physical properties such as thermal conductivities and specific heat capacities are not a function of temperature;
- water vapor adsorbed by the zeolite beads is supposed in liquid phase and in thermal and chemical equilibrium with the solid material;
- at the outlet of the experimental bench, it is assumed that pressure of the air flow is equal to the atmospheric pressure.

With the above assumptions, the proposed model consists of conservative equations of heat and mass transfer on each phase (humid air, zeolite beads), and a kinetic equation based on solid-vapor sorption interactions. To solve the mentioned equations, the finite volume method is used and the sorption bed is divided into a number of segments of equal thickness. For each segment, energy balances are formulated for the air flow and for the zeolite beads. The resulting system of discretized equations is solved by the DASSL integration algorithm of Dymola solver (Dassault Systems AB., 2011).

2.2. Governing equations of the model

Equations expressing the mass balances in the reactor are based on the laws of mechanics flow in porous media (Duval F. et al., 2004, Hager J. et al, 2000, Nield D. A. and Bejan A., 1999, Sozen M. and Vafai K., 1990). They are the following:

- Mass balance for the fluid phase

$$\frac{\partial(\xi_l \rho_{ah})}{\partial t} + \nabla[\rho_{ah}.u] + (1-\xi_t)\rho_z \frac{\partial X_z}{\partial t} = 0 \qquad \text{(eq.1)}$$

where $\xi_l \rho_{ah}$ is the apparent humid air density, $\nabla[\rho_{ah}.u]$ the mass balance and $(1-\xi_t)\rho_z \frac{\partial X_z}{\partial t}$ the sorption source term (positive or negative given the sorption phase, adsorption or desorption). Equation (1) is rewritten for water vapour only as follows:

$$\xi_l \rho_{ah} \frac{\partial(X_{ah})}{\partial t} + (\rho_{ah} u)\nabla[X_{ah}] + (1 - X_{ah})(1 - \xi_t)\rho_z \frac{\partial X_z}{\partial t} = 0 \quad \text{(eq.2)}$$

- Momentum equation

The velocity of the fluid flow along the bed axis is determined by using the following Darcy's equation (inertial effects are assumed negligible compared to viscous effects, given the low average value of the Knudsen number of the sorption considered bed - Kn = 9.5 x 10^{-5}):

$$u = -\frac{\xi_l^3 . d_p^2}{120.(1 - \xi_l)^2 . \mu_{ah}} \nabla P \quad \text{(eq.3)}$$

where parameters d_p and μ_{ah} are respectively the particle diameter and the air flow dynamic viscosity.

- Energy conservation equation for the fluid phase

Heat transfer inside the fluid phase in the sorption bed is described as follows:

$$\xi_l \frac{\partial\left(\rho_{ah} c_{v,ah} T_{ah}\right)}{\partial t} = a_v h_{conv,ah,z}(T_z - T_{ah}) + u.\nabla\left[\rho_{ah} c_{p,ah} T_{ah}\right] + A_{ah,p} h_{conv,ah,p}\left(T_{ah} - T_p\right) \quad \text{(eq.4)}$$

where $\left(\rho_{ah} c_{v,ah} T_{ah}\right)$ is the internal energy of the fluid phase, $a_v h_{conv,ah,z}(T_z - T_{ah})$ the convective heat transfer between the zeolite beads and the air flow, $u.\nabla\left[\rho_{ah} c_{p,ah} T_{ah}\right]$ the enthalpy balance of the fluid phase, and $A_{ah,p} h_{conv,ah,p}\left(T_{ah} - T_p\right)$ the heat exchange between the air flow and the wall of the reactor. The zeolite beads specific surface area (a_v, m^2/m^3) is determined by the correlation (Holdich R.G., 2002):

$$a_v = (1 - \xi_l) * \frac{6}{d_p} \quad \text{(eq.5)}$$

The heat transfer coefficient ($h_{conv,ah,z}$) between air and the zeolite beads can be described by Dittus and Boelter's equation (Bejan A., 1995, Mhimid A., 1998):

$$h_{conv,ah,z} = \frac{k_{ah}}{d_{pb}}(2 + 1.8 * Pr^{0.33} * Re^{0.5}) \qquad \text{with} \qquad Pr = \mu_{ah}.c_{p,ah}/k_{ah} \quad \text{(eq.6)}$$

Volumetric heat capacities of the fluid phase can be determined using the following correlations:

$$c_{v,ah} = X_{ah}.c_{v,v} + (1 - X_{ah}).c_{v,as} \quad ; \quad c_{p,ah} = X_{ah}.c_{p,v} + (1 - X_{ah}).c_{p,as} \quad \text{(eq.7)}$$

where $c_{v,ah}$ (resp. $c_{p,ah}$) is the volumetric heat capacity at constant volume (resp. at constant pressure) of humid air.

- Energy conservation equation for the solid phase

Heat transfer inside the zeolite beads is described as follows:

$$\rho_z(1 - \xi_t)\left(c_{pz} + X_z c_{pw}\right)\frac{\partial(T_z)}{\partial t} = \nabla.[k_z \nabla \mathrm{T}_z] + a_v h_{conv,ah,z}(T_z - T_{ah}) + (1 - \xi_t)\rho_z \frac{dX_z}{dt} Q_R \quad \text{(eq.8)}$$

where $\nabla.[k_z \nabla \mathrm{T}_z]$ represents the conduction heat transfer, $a_v h_{conv,ah,z}(T_z - T_{ah})$ the convective heat transfer with the fluid phase and $(1 - \xi_t)\rho_z \frac{dX_z}{dt} Q_R$ the heat source/sink term. The heat exchange between the zeolite beads and the reactor walls is assumed negligible compared to other transfers, given the low particles contact area with the reactor walls.

2.3. Sorption kinetics

The performance of such systems is largely determined by the kinetics of the processes in the zeolite bed. The LDF model (originally proposed by Gleuckauf et al., 1947) can be used to determine the sorption rate or internal mass transfer inside the porous media for systems with long characteristic times ($\frac{D_e}{d_p^2} > 10^{-3}$, which is the case here with a value of less than 10^{-4}) (Chahbani M. et al, 2002). The mass transfer resistance from the adsorbate phase into the micro-pores of the zeolite beads is reduced to an overall mass transfer resistance k_m as described in the following correlation :

$$\frac{\partial(X_z)}{\partial t} = k_m.\left(X_{eq} - \mathrm{X}_z\right) \quad \text{(eq.9)}$$

with $k_m = k_o \frac{D_e}{d_p^2}$ $D_e = D_o \exp\left(-\frac{E_a}{RT_z}\right)$ (eq.10)

The zeolite's water mass fraction at equilibrium is determined using a polynomial fitting approximation of measured sorption isotherms (Bales et al., 2005) over a wide range of temperature and partial water vapour pressure range:

$$X_{eq} = (a_2.T_z^2 + a_1.T_z + a_0) + 0.0228 * \ln\left[\frac{P_v}{P_{sat}}\right] \quad \text{(eq.11)}$$

with a_2=3E-06 K^{-2}, a_1=-0.0017 K^{-1}, and a_0=0.3206. The water vapour partial pressure (P_v) is determined using the Dalton law as follows (Ravi R.,2011):

$$P_v = \left(\frac{14.X_{ah}}{9 + 5.X_{ah}}\right).P_{ah} \quad \text{(eq.12)}$$

P_{sat} is estimated using the Dupre correlation (-50°C - + 200°C) (Jannot Y., 2005):

$$P_{sat} = 133.322 * \exp\left[46.784 - \frac{a_3}{T_z} - 3.868\ln(T_z)\right] \quad \text{(eq.13)}$$

with a_3=6435 K.

2.4. Isotherms equations

A polynomial fitting approximation to the experimental curves from (Bales et al., 2005) of measured heat of adsorption (at 40 °C and 90 °C) of the zeolite 13X/H_2O couple was used to determine the expression of the heat of adsorption Q_R at water loading X_z:

$$Q_R = b_5.X_z^5 + b_4.X_z^4 + b_3.X_z^3 + b_2.X_z^2 + b_1.X_z + b_0 \quad \text{(eq.14)}$$

with b_5=8.4E+06 J/g, b_4=-6.1E+06 J/g, b_3=1.41E+06 J/g, b_2=-7.3E+04 J/g, b_1=-1.5E+04 J/g and b_0=4124 J/g.

3. Experimental setup

A reactor test bench was developed to validate the above-presented model. The bench consists of two cylindrical vessels of 140 liters, filled with zeolite beads of 2 mm diameter, disposed over the entire section of the bed (0.48 m^2) at an height of 20 cm. To be able to test the zeolite vessels under various operating conditions (flow rate and variable humidity), the bench is designed with a modular configuration as shown in Figure 2. The parallel configuration, with valves V1, V2, V3, V5, V6 and V7 open and valve V4 closed, allows to observe the sorption behavior of both vessels and to have a comparison of their thermochemical performances. The series configuration is obtain with the valves V1, V3, V4, V6 and V7 open and valves V2 and V5 closed. This configuration allows to observe the effect of the upstream vessel M1 on the sorption behavior of M2.

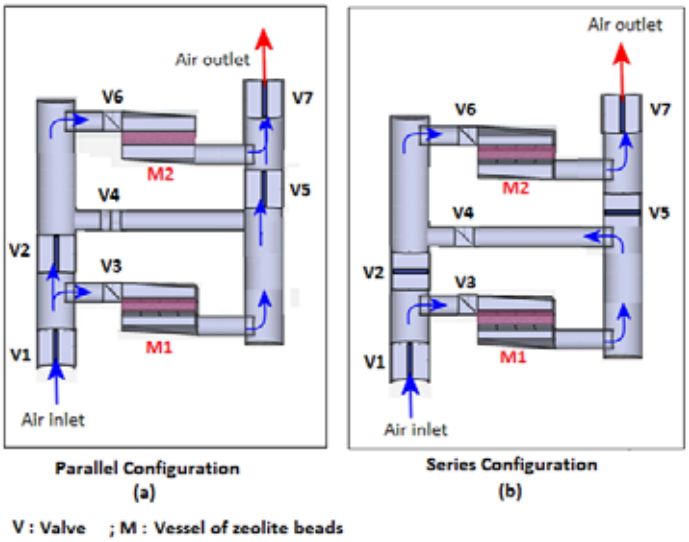

Fig. 2 : Schematic of the experimental bench (CETIAT, 2014)

Valves V1 and V7 maintain the air tightness of the device during off periods. Figure 3 shows a picture of the experimental bench as built. The thermal insulation of each vessel is made of a 5 cm thick layer of glass wool (0.8 W/(m.K)). The sealing at the contact surfaces between the various zones of each module is provided by grout resistant to high temperatures. The air is always flown downwards in the vessels, to ensure mechanical stability of the beds over the successive absorption/desorption cycles.

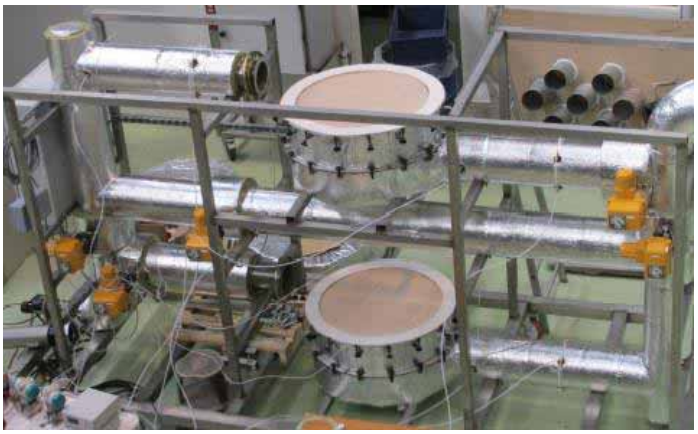

Fig. 3: Picture of the experimental bench with open and filled vessels (CETIAT, 2014)

3.1.Instrumentation

Table 1 shows a list of the main measurement sensors used during the experimental investigations. The temperatures profile of the airflow at the inlet and the outlet of each zeolite vessel is measured with type K thermocouples (± 0.1 K, see Table 1). Before testing, all thermocouples have been calibrated and adjusted. The pressures of the airflow at the same positions are obtained from differential type DT-ULP sensor, with an accuracy of 0.25%. Volume flow rates of the air at the inlet and the outlet of the experimental bench are measured with an ultrasonic flow meter (with an accuracy of 0.3%). During the discharging phase, the air humidity upstream and downstream of each zeolite vessel is measured with a chilled mirror hygrometer with an accuracy of 0.3% -0.8% over the dew point temperature range of [-40°C-20°C]. Since this hygrometer is not suitable high temperatures airflows (> 90°C), these humidity measurements are only conducted upstream of the heat source during the charging phases.

Table 1: List of the main measurement sensors of the experimental bench

Sensor	Specifications

Thermocouple type K type : TPI A	- range : 0 – 200 °C - accuracy : ± 1°C
Ultrasonic flow meter	- range : 10 m^3/h -750 m^3/h - accuracy : 0.3 %
Differential pressure sensor type : DT-ULP	- range : ± 500 Pa - accuracy : 0.25 %
Chilled mirror hygrometer	- range : - 65 °C à + 25 °C - accuracy : 0.3%-0.8%

3.2.Measurement campaign

Table 2 presents a description of some of the tests that have been conducted on the bench. For each of the 2 working configurations of the experimental bench previously described, a charging phase followed by a discharging phase is conducted according to the following specifications:

- during the discharging phase, a stream of hot air (120 to 180 °C, ambient humidity, 180 m^3/h) is flown at the inlet of the experimental bench to perform the desorption of water from zeolite beads;
- during the charging phase, a cold and humid air stream (20 °C, 10 g/kg as , 180 m^3/h) is circulated at the inlet of the experimental bench. The air is dried and heated by the adsorption phenomenon.

These specifications were chosen to represent real conditions that could be observed in a storage system connected to solar collectors and a building, as described in (Tatsidjodoung, 2014). For all experiments, the reactors were filled with 40 kg of dry zeolite. The bulk density of zeolite beads is calculated to ρ = 690 kg/m^3, assuming a porosity of ε_p = 0.42 and a fix bed porosity of ε_l = 0.39.

Table 2: Measurement campaign conditions

Configuration	Designation	Type	Inlet air temperature (°C)	Volume flowrate (m^3/h)	Relative humidity of inlet air (%)
M1 and M2 in parallel	Test 1	charging	180	180	Ambiant
	Test 2	discharging	20		70
M1 and M2 in series	Test 3	charging	120	180	Ambient
	Test 4	discharging	20		70

4. Results: model validation and reactor analysis

Table 3 presents the main parameters used in the numerical simulations. Without an experimental characterisation of the sorption kinetic of the used sorbent, the reference mass transfer resistance coefficient (k_o) has been varied until good agreement between measured and calculated temperatures and air humidity profiles in the reactors were obtained. The numerical model is very sensitive to this parameter. Good agreement between experiment and simulation results has been obtained for a value of 2 x 10^5 s^{-1} for the reference mass transfer coefficient.

Table 3: Model input parameters

Parameter		**Unit**	**Value**	**Reference**
Zeolite beads density	ρ_z	kg/m^3	960	
Zeolite bulk thermal conductivity	λ_z	W/(m.K)	0.20	Breck D. W., 1964
Bed porosity	ε_l		0.39	Ergun S., 1952
Zeolite beads porosity	ε_p		0.42	Ergun S., 1952

particle diameter		d_p	mm	2	Experiment
Activation energy		E_o	J/mol	2.95 x 10^4	Breck D. W., 1964
Reference diffusivity		D_o	m^2/s	0.02 x 10^{-4}	Breck D. W., 1964
Specific heat capacity of the zeolite		C_{pz}	J/(kg.K)	900	Breck D. W., 1964
Total mass of zeolite beads		M_z	kg	40	Experiment
Specific heat capacity of the bed's wall		C_{pm}	J/(kg.K)	450	
Density of the bed's wall		ρ_m	kg/m^3	8010	
Thickness of the bed's wall		e_m	mm	2	Experiment
Thickness of the bed's insulation		e_i	mm	50	Experiment
Thermal conductivity of the bed's insulation		λ_i	W/(m.K)	0.08	
Number of axial nodes		N		5	
Initial temperature		T_o	°C	25	Experiment
Initial water mass fraction of zeolite beads for	Test 1	X_{zo}	kg/kg	0.24	Ceca Arkema Group, 2008
	Test 2			0.03	
	Test 3			0.24	Ceca Arkema Group, 2008
	Test 4			0.06	
Initial water mass fraction of air volume inside bed's macropores		X_{ah}	kg/kg	0.001	

4.1. Charging test

Figures 4 and 5 show a comparison between experimental and numerical results for the temperature of the airflow at the outlet of vessels M1 and M2 during the discharging tests 1 and 3. A good agreement is obtained, confirming thus the good approximation of the LDF model. Test 1 (resp. test 3) is performed with M1 and M2 in parallel (resp. M1 and M2 in series), an airflow inlet temperature of 180 °C (resp. 120°C) and a volume flow rate of 180 m^3/h. At the beginning, the zeolite beads are supposed saturated with water, corresponding to water mass fraction of 0.24. An analysis of the temperature profiles shows that 3 phases can be observed during the desorption process inside the vessels:

- Phase 1: During this phase (lasting approximately 1/2h), the temperature of the air at the outlet equals the initial temperature of the zeolite beads (~20°C). The heat provided by the incoming air is absorbed by the desorption process in the top layers of the bed.
- Phase 2: This phase (lasting up to 2h) is characterized by a small jump followed by a plateau at 35-40°C of the air temperature at the outlet of the vessels. It is a consequence of the re-condensation process in the bottom layers of the bed of the water desorbed in the top layers. As the airflow exiting the top of the bed is saturated with vapor, its cooling as it flows through the zeolite beads located at the bottom of the bed causes a re-condensation of a fraction of the vapor previously desorbed. The heat released by this phenomenon causes an increase of the exit air temperature.
- Phase 3: This last phase occurs when the temperature of the zeolite beads inside the whole reactor is higher than the wet bulb temperature of the vapor-saturated airflow exiting the bed. As a consequence, the outlet temperature of the airflow remains constant until the sorption front has crossed the bottom layers of the zeolite bed, which results in an increase of the outlet temperature of the airflow.

Another result from Figure 4 concerns the unequal distribution of the airflow between M1 and M2. M1 seems to be crossed by an airflow at a lower rate than M2 as its sorption duration is 2h longer than that of M2. Also, the difference between the inlet and the outlet temperatures at the end of the desorption process shows the existence of different heat losses through the bench's different walls. In consequence, as it can be seen in Figure 5, the temperature of zeolite beads in vessel M2 at the end of the desorption process (105 °C) is lower than in M1 (120 °C) due to thermal losses in the pipes between the two vessels when air is circulated

in series. This results, at the end of the corresponding charging process, in the water mass fraction of the zeolite beads in vessel M2 higher than that of zeolite beads in vessel M1.

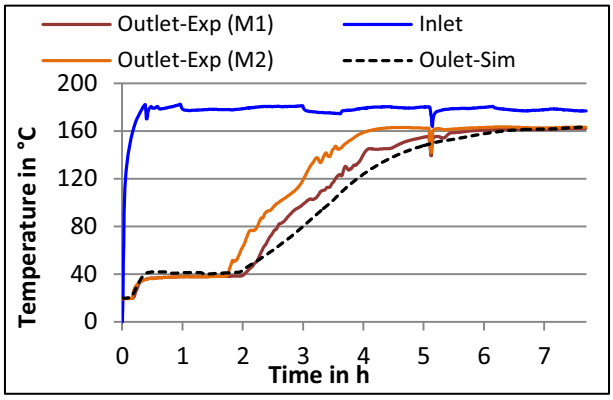

Fig. 4 : Measured and simulated temperature at the inlet and outlet of vessels M1 and M2 during test 1

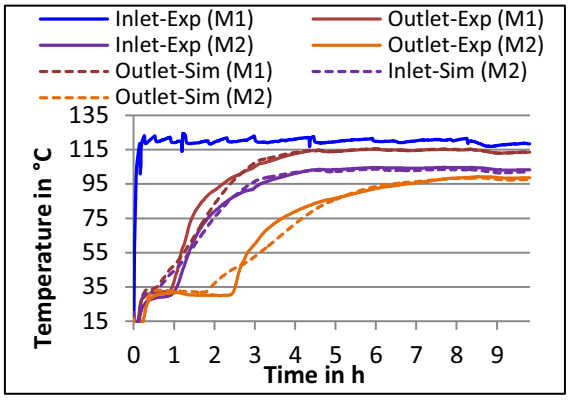

Fig. 5: Measured and simulated temperature at the inlet and outlet of vessels M1 and M2 during test 3

4.2. Discharging test

Following the charging tests, a discharging of the vessels is conducted for each of the tested configurations with an airflow at a temperature of 20 °C, a specific humidity of 10 g/kg as and a volume flow rate of 180 m^3/h. Figures 6 to 9 show a comparison between experimental and numerical results for the temperature and the specific humidity of the air at the outlet of vessels M1 and M2 during the discharging tests 2 and 4. A good agreement is obtained, confirming thus the good approximation under the LDF model assumption.

For both tests, the maximum temperature rise of the airflow at the outlet of the vessels is 38 °C, with a longer discharging time for test 2. A higher charging temperature (180°C for test 1 and 120°C for test 3) and a lower flow rate (split in 2 due to the parallel configuration during test 2) of the air crossing the vessels during discharging both explain the higher discharging time observed for test 2. Figure 6 shows a faster fall of the air temperature at the outlet of vessel M2 during test 2, which implies that vessel M2 is flown by an airflow at a higher flow rate than vessel M1. This explanation also applies to the humidity of the air at the outlet of the vessels shown on Figure 8. This difference, also observed during the charging tests as said before, is due to different pressure losses in the two vessels even though the zeolite beads are identical and the charging process procedures were strictly followed for both of them.

The results on the specific humidity of the airflow (Figures 8 and 9) show that for both tests almost all the water contained in the air is adsorbed by zeolite beads during the first hours of the experiments; which illustrates the high affinity of zeolite towards water vapor. Results from test 4 (Figure 7) show that the temperature of the air at the outlet of the experimental bench with vessels in series is at its maximum (58 °C) during vessel M2 adsorption period (time > 3.5 h). As a matter of fact, a significant part of the heat generated during the adsorption process inside vessel M1 is also used to heat up the zeolite beads of both vessels (up to the adsorption temperature) and some is also dissipated to the surroundings.

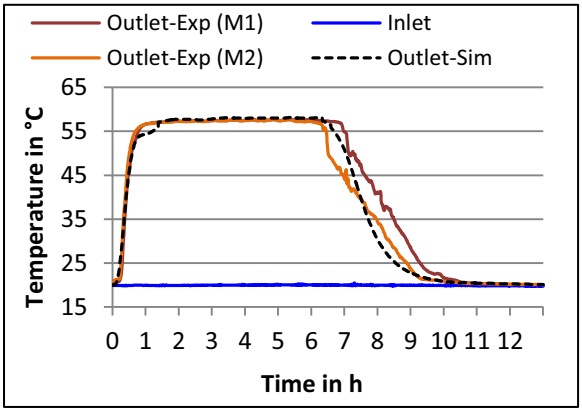

Fig. 6: Measured and simulated temperature at the inlet and outlet of vessels M1 and M2 during test 2

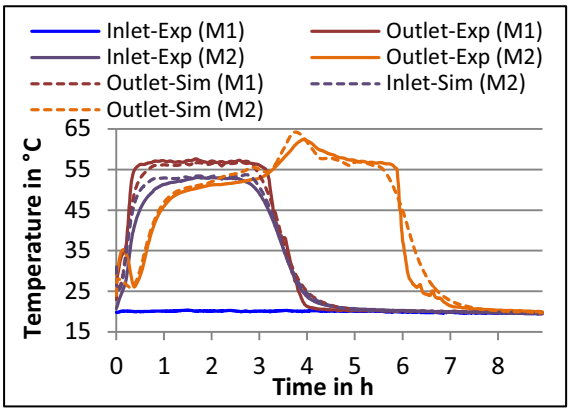

Fig. 7: Measured and simulated temperature at the inlet and outlet of vessels M1 and M2 during test 4

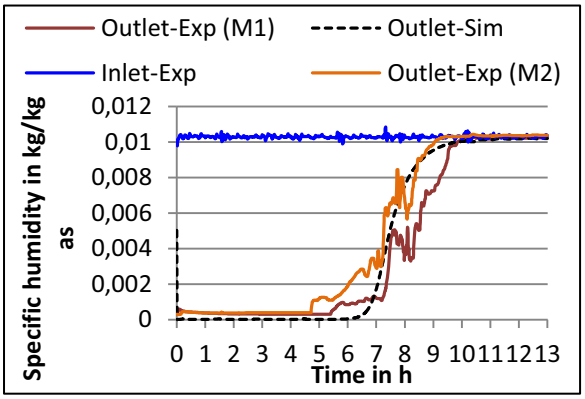

Fig. 8: Measured and simulated specific air humidity at the inlet and outlet of vessels M1 and M2 during test 2

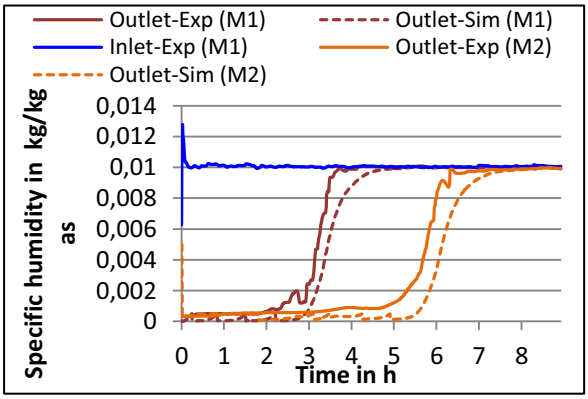

Fig. 9: Measured and simulated specific air humidity at the inlet and outlet of vessels M1 and M2 during test 4

5. Conclusion

A numerical and experimental study of the evolution of a zeolite based thermochemical reactor is presented. Results show that the temperature reached by the air exiting the storage reactor (>55°C) under typical operating conditions that could be observed in a building are appropriate for building heating. The desorption of the reactor at a temperature as low as 120°C is possible, thus the use of a solar collector to heat up the reactor during the charging phase can be foreseen, even though a desorption at a temperature higher than 150°C will allow a higher storage density oft he system. The simulation results fit correctly the experimental results, thus this model could be used to simulate the system evolution when coupled to a solar building.

6. Nomenclature

A	heat exchange surface, m^2
a_v	specific surface area solid – gas, m^2/m^3
c_p	specific heat capacity at constant pressure, $J/(kg.K)$
c_v	specific heat capacity at constant volume, $J/(kg.K)$
D_e	equivalent diffusivity in the adsorbent particles, m^2/s
D_o	reference diffusivity, m^2/s
d_p	diameter of zeolite beads, m
$\overline{d_{pb}}$	average pore diameter, m
Q_R	heat of adsorption, $J/g\ of\ water$
E_a	activation energy, J/mol
h_{conv}	convection heat exchange coefficient, $W/(m^2.K)$
K_{ck}	constant of Carman-Kozeny
k_m	mass transfer coefficient within the adsorbent

Greek symbols

ξ	porosity
ρ	density, (kg/m^3)
μ	dynamic viscosity $(Pa.s)$

Sub- and super-scripts

ah	humid air
as	dry air
eq	equilibrum
p	wall
sat	saturation
t	total
v	water vapor
w	liquid water

	particles, *1/s*		
k	thermal conductivity, *W/(m.K)*	z	zeolite
Kn	Knudsen number		
m	mass, *kg*		
P	pression, *Pa*		
Pr	Prandtl number		
Re	Reynolds number		
T	temperature, *K*		
u	velocity, *m/s*		
X	water mass fraction, *kg of water/kg de compound*		

7. Acknowledgements

This project has been performed in the framework of the STAID project, financed under ref. ANR-2010-STKE-009-05 by the French National Research Agency (ANR).

8. References

Bales C., Gantenbein P., Hauer A., Henning H.-M., Jaenig D., Kerskes H., 2005. Thermal properties of materials for thermo-chemical storage of solar heat. 20 p. Report no.B2-Task 32. available at: http://www.iea-shc.org/publications/downloads/task32-Thermal_Properties_of_Materials.pdf.

Bejan A., 1995. Convection Heat Transfer. 2nd ed. John Wiley & Sons;New York.

Breck D. W., 1964. Zeolite Molecular Sieves. New York.John Wiley and Sons.

Ceca Arkema Group, 2008. Siliporite molecular sieves. March. available at: http://www.cecachemicals.com/en/expertise/molecular-sieves/natural-gas/index.html.

Centre Technique des Industries Aérauliques et Thermiques (CETIAT), 2014.http://www.cetiat.fr/.

Chahbani M. H., Labidi J., Paris J., 2002. Effect of mass transfer kinetics on the performance of adsorptive heat pump systems. Applied Thermal Engineering;22:23-40.

Dassault Systèmes AB. November 2011. User Manual. Dymola (Dynamic Modeling Laboratory). 558 pages.

Duval F., Fichot F., Quintard M., 2004. A local thermal non-equilibrium model for two-phase flows with phase-change in porous media. International Journal of Heat and Mass Transfer;47:613-639.

Ergun S., 1952. Fluid flow through packed columns. Chemical Engineering Progress;48:89-94.

Glueckauf E., Coates J. I., 1947. 241. Theory of chromatography. Part IV. The influence of incomplete equilibrium on the front boundary of chromatograms and on the effectiveness of separation. Journal of the Chemical Society (Resumed) 1315-1321.

Hager J., Wimmerstedt R., Whitaker S., 2000.Steam drying a bed of porous spheres: Theory and experiment. Chemical Engineering Science;55:1675-1698.

Holdich R.G., 2002. Fluid flow through porous media. Fundamentals of Particle Technology. Midland Information Technology and Publishing,;. 173 pages.

Jannot Y., 2005. L'air humide, online course available at: http://www.thermique55.com/principal/airhumide.pdf

Mhimid A., 1998. Theoretical study of heat and mass transfer in a zeolite bed during water desorption: validity of local thermal equilibrium assumption. International Journal of Heat and Mass Transfer;41:2967-2977.

Nield D. A., Bejan A. 1999. Convection in Porous Media. Springer.

Ravi R.,2011. The Gibbs-Duhem Equation, the Ideal Gas Mixture, and a Generalized Interpretation of Dalton's Law. Industrial & Engineering Chemistry Research;50:13076-13082.

Sozen M., Vafai K. 1990. Analysis of the non-thermal equilibrium condensing flow of a gas through a packed bed. International Journal of Heat and Mass Transfer;33:1247-1261.

Tatsidjodoung P., Le Pierres N., Luo L., 2013. A review of potential materials for thermal energy storage in building applications, Ren. and Sust. En. Rev., 18, 327-349.

Tatsidjodoung P., 2014, Procédé de stockage d'énergie solaire thermique par adsorption pour le chauffage des bâtiments : Modélisation et Simulation numérique, PhD thesis, Université de Savoie.

Yu N., Wang R. Z., Wang L. W., 2013. Sorption thermal storage for solar energy. Progress in En. and Comb. Sc., 39, 489-514.